Magazine of Concrete Research
Volume 65 Issue 2

Performance of a DSCT column under lateral loading: analysis
Han, Won, Kim and Kang

Magazine of Concrete Research, 2013, **65**(2), 121–135
http://dx.doi.org/10.1680/macr.12.00024
Paper 1200024
Received 18/10/2011; revised 23/05/2012; accepted 13/07/2012
Published online ahead of print 21/11/2012

ice
Institution of Civil Engineers
publishing

Performance of a double-skinned composite tubular column under lateral loading: analysis

Taek Hee Han
Senior Research Scientist, Coastal Development & Ocean Energy Research Division, Korea Institute of Ocean Science and Technology, Ansan, Republic of Korea

Deok Hee Won
Researcher, Coastal Development & Ocean Energy Research Division, Korea Institute of Ocean Science and Technology, Ansan, Republic of Korea

Seungjun Kim
Postdoctoral Research Associate, Texas Transportation Institute, Texas A&M University, College Station, Texas, USA

Young Jong Kang
Professor, School of Department of Architectural, Civil and Environmental Engineering, Korea University, Seoul, Republic of Korea

An analytical model of a double-skinned composite tubular (DSCT) column was developed and verified using test results. The experimental results demonstrated the rigour and the validity of the present analytical model. Brief parametric studies were carried out for DSCT columns. The developed model considered the confining effect and material non-linearity of concrete. By the buckling or yielding condition of the inner tube of a DSCT column, its failure mode and concrete model were defined. The strength of concrete, the hollow ratio of a DSCT column, and the thickness of an inner tube were selected as the main parameters that affect the behaviour of a DSCT column. The analysis results showed that concrete strength and the thickness of the inner tube affect the axial strength and moment capacity of the column, while the hollow ratio affects only its axial strength.

Notation

$A_{i,j}^{CC}$ cross-sectional area of the jth element of the concrete at the ith stage of strain distribution
$A_{i,j}^{IT}$ cross-sectional area of the jth element of the inner tube at the ith stage of the strain distribution
$A_{i,j}^{OT}$ cross-sectional area of the jth element of the outer tube at the ith stage of the strain distribution
C_b distance from the neutral axis to the near outer surface
$C_{b.i}$ distance from the neutral axis to the near outer surface at the ith stage of the strain distribution
D outer diameter of confined concrete
D_i diameter of hollow section or inner diameter of confined concrete
E modulus of elasticity
E_c tangent modulus of unconfined concrete
E_{ity} modulus of elasticity of inner tube
E_{oty} modulus of elasticity of outer tube
E_{sec} secant modulus of unconfined concrete
e_b balanced eccentricity
F lateral force or lateral load
$F_{L,i}$ lateral force at the ith stage of the strain distribution
f_{bk} buckling strength of the inner tube
f_c stress acting on concrete
f_{co} strength of unconfined concrete
f_{cc} confined strength of concrete
f_{it} stress acting on the inner tube
$f_{i,j}^{CC}$ stress acting on the jth element of the concrete at the ith stage of the strain distribution
$f_{i,j}^{IT}$ stress acting on the jth element of the inner tube at the ith stage of the strain distribution
$f_{i,j}^{OT}$ stress acting on the jth element of the outer tube at the ith stage of the strain distribution
f_{ity} yield strength of the inner tube
f_l confining pressure
f_{lc} confining pressure in the circumferential direction
f_{lr} confining pressure in the radial direction
f_{ot} stress acting on the outer tube
f_{oty} yield strength of the outer tube
f_s stress acting on steel
$f_s(\varepsilon_s)$ stress function of steel
f_u ultimate stress of steel
f_y yield stress of steel
h height of the column
L_p length of the plastic hinge
$L_{p,i}$ length of the plastic hinge at the ith stage of the strain distribution
M moment
M_0 nominal moment without axial load
M_b nominal moment under balanced condition
M_i moment at the ith stage of the strain distribution
M_i^{CC} moment acting on concrete at the ith stage of the strain distribution
M_i^{IT} moment acting on the inner tube at the ith stage of the strain distribution
M_i^{OT} moment acting on the outer tube at the ith stage of the strain distribution

$M_{i,j}^{CC}$ moment acting on the jth concrete element at the ith stage of the strain distribution
$M_{i,j}^{IT}$ moment acting on the jth inner tube element at the ith stage of the strain distribution
$M_{i,j}^{OT}$ moment acting on the jth outer tube element at the ith stage of the strain distribution
M_n nominal moment capacity of the column
M_u maximum moment capacity of the column
M_y yield moment of the column
$M(z)$ moment function
N_e axial strength by empirical model (Wei *et al.*, 1995b)
N_p axial strength by the developed model (present)
N_s summation of each axial strength (inner tube, outer tube, concrete)
N_t axial strength from test (Wei *et al.*, 1995a)
P axial load
P_0 nominal axial strength without eccentricity
P_b nominal axial strength under balanced condition
P_i axial load at the ith stage of the strain distribution
P_i^{CC} axial load acting on core concrete at the ith stage of the strain distribution
P_i^{IT} axial load acting on inner tube at the ith stage of the strain distribution
P_i^{OT} axial load acting on outer tube at the ith stage of the strain distribution
$P_{i,j}^{CC}$ axial load acting on the jth concrete element at the ith stage of the strain distribution
$P_{i,j}^{IT}$ axial load acting on the jth inner tube element at the ith stage of the strain distribution
$P_{i,j}^{OT}$ axial load acting on the jth outer tube element at the ith stage of the strain distribution
p_n axial load applied on neutral axis
$S_{i,j}$ length of the jth column element at the ith stage of the strain distribution
t_c thickness of the concrete wall
t_i thickness of the inner tube
t_o thickness of the outer tube
t_{bk} required minimal thickness of the inner tube to avoid its buckling failure
t_{eq} equivalent thickness of the corrugated inner tube
t_{yt} required minimal thickness of the inner tube to avoid its yielding failure
w_f height of the wave
w_l length of one-half a wave
w_S arc-length of one-half a wave
$x_{i,j}^{CC}$ distance from neutral axis to the centre of jth concrete element at the ith stage of the strain distribution
$x_{i,j}^{IT}$ distance from neutral axis to the centre of jth inner tube element at the ith stage of the strain distribution
$x_{i,j}^{OT}$ distance from neutral axis to the centre of jth outer tube element at the ith stage of the strain distribution
z distance from the bottom of the column to a specific point along the height
Δ lateral displacement
Δ_i lateral displacement of the column at the ith stage of the strain distribution
$\Delta_{i,j}$ lateral displacement of the jth column element at the ith stage of the strain distribution
ε axial strain of concrete
ε_{cc} axial strain of concrete at its peak strength
ε_{co} axial strain of unconfined concrete at its peak strength
ε_{cu} ultimate strain of the concrete
$\varepsilon_{L,i}$ strain of left end in the critical section at the ith stage of the strain distribution
$\varepsilon_{R,i}$ strain of right end in the critical section at the ith stage of the strain distribution
ε_s strain of steel
ε_u ultimate strain of the steel
ε_y yield strain of the steel
$\theta_{i,j}$ rotation angle of the jth column element at the ith stage of the strain distribution
ϕ_i curvature of the column at the ith stage of the strain distribution
$\phi(z)$ curvature function

Introduction

Double-skinned composite tubular (DSCT) columns have been studied by many researchers (Tao *et al.*, 2004; Wei *et al.*, 1995a, 1995b; Zhao and Grzebieta, 2002) and a double-skinned hybrid tubular (DSHT) column, which is composed of a fibre-reinforced-polymer (FRP) tube and a steel tube, has also been investigated (Teng *et al.*, 2006; Yu *et al.*, 2006). Many researchers agree that a DSCT or DSHT column member shows strength greater than the sum of the strengths of each component, but these studies have focused on only the axial strength enhancement of a DSCT column. In this study, an analytical model of a DSCT column is proposed using section analysis and a curvature function. The developed model adopted the definition of failure mode and the nonlinear concrete model for a DSCT column that were suggested by Han *et al.* (2010). The proposed model predicted the behaviour of a DSCT column with acceptable accuracy through the axial load–bending moment (P–M) interaction, lateral load–lateral displacement (F–Δ) relation, yield strength, ultimate strength, yield displacement, ultimate displacement, yield energy, ultimate energy, and the ductility factors. This paper presents the first analytical study on the behaviour of a DSCT column under lateral loading.

Analytical model

Material model

For the development of a nonlinear DSCT column model, the definition of failure mode and nonlinear concrete model proposed by Han *et al.* (2010) were adopted. The failure modes of a DSCT column are categorised into three cases (Han *et al.*, 2010). The failure mode governs the confined states of concrete, which are the triaxially confined state, the biaxially confined state, and the unconfined state. The first failure mode happens when the inner tube fails by buckling or yielding before the outer tube yields. In the second failure mode, the outer tube fails before the inner tube

fails. The third failure mode is the case when the inner and outer tubes fail simultaneously. In the first failure mode, the concrete of a DSCT column is in the state of triaxial confinement before the inner tube fails. After the failure of the inner tube, the inner tube will no longer exert any confining pressure. In the second failure mode, the concrete is triaxially confined before yielding or buckling failure of the outer tube. In the third failure mode, the concrete is again triaxially confined before the DSCT column fails. In the third failure mode, a DSCT column would fail brittlely. Therefore, the concrete in a DSCT column has various stress–strain curves by its failure mode. When an axial load is applied only on the concrete of a DSCT column, the inner and outer tubes provide passive confining stress according to the Poisson effect. Therefore, the concrete wall element between the inner and outer two tubes is under triaxial confinement unless one of the two tubes fails. If the inner tube yields or is buckled, the passive confining stress will not exist. Therefore, the concrete wall element is under biaxial confinement. If the outer tube yields due to the passive confining stress, there will be no confining stress and the DSCT column is supposed to fail.

The equilibria of failure modes II and III are expressed as Equations 1 and 2, respectively (Han *et al.*, 2010). They were derived from the free body diagram shown in Figure 1 when an axial load was applied only on the concrete until the outer tube yielded by lateral pressure induced by the Poisson's effect. When the concrete in a DSCT column is triaxially confined, f_{lc} and f_{lr} are equal. Therefore, they can be substituted by f_l as shown in Equations 1 and 2. By substituting Equation 2 into Equation 1, Equation 3 is derived. The stress acting on the inner tube (f_{it}) is given as Equation 4 by substitution of Equation 3 into Equation 2.

$$f_{lc}(D - D_i) + 2f_{it}t_i = f_l(D - D_i) + 2f_{it}t_i$$
$$= f_lD - f_lD_i + 2f_{it}t_i$$
$$= 2f_{ot}t_o \quad (1)$$

$$f_{lr}D_i = f_lD_i = 2f_{it}t_i \quad (2)$$

$$f_l = \frac{2f_{ot}t_o}{D} \qquad f_lD = 2f_{ot}t_o \quad (3)$$

$$f_{it} = \frac{f_lD_i}{2t_i} = \frac{t_oD_i}{t_iD}f_{ot} \quad (4)$$

f_{it} has the maximum value when f_{ot} is equal to f_{oty}. To avoid the yielding failure of the inner tube before the outer tube yields, f_{it} must be less than f_{ity}. This yielding condition of the inner tube can be defined as in Equation 5. Therefore, the required minimal thickness of the inner tube to avoid its premature yielding failure (t_{yt}) is expressed as Equation 6 (Han *et al.*, 2010).

$$f_{it} = \frac{t_oD_i}{t_iD}f_{oty} < f_{ity} \quad (5)$$

$$t_{yt} = \frac{f_{oty}D_i}{f_{ity}D}t_o \quad (6)$$

Han *et al.* (2010) proposed the buckling strength of the inner tube (f_{bk}) as in Equation 7. Because the inner tube is unilaterally restrained by concrete, it has a different buckled shape and buckling strength from those of an arch or a ring which has bilateral boundary conditions. Han *et al.* (2010) assumed that the buckled shape was similar to that of a shallow arch, which showed snap-through buckled shape. For this reason, they adopted the snap-through buckling load coefficient that was proposed by Kerr and Soifer (1969). Using the safety condition that f_{bk} (Equation 7) should be larger than f_l (Equation 3), the required

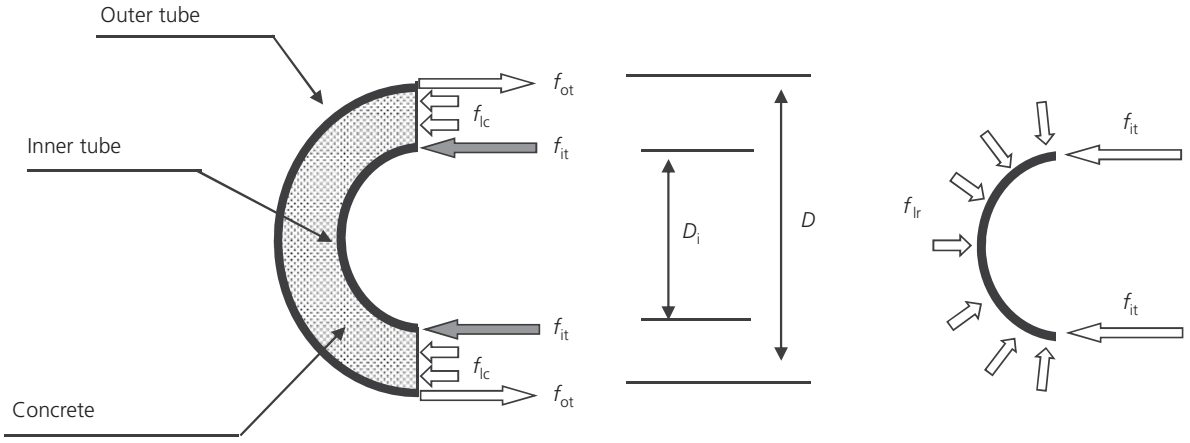

Figure 1. Confining stress on concrete in a DSCT column

minimal thickness of the inner tube to avoid buckling failure (t_{bk}) is given as Equation 8 (Han *et al.*, 2010). To avoid the buckling failure of the inner tube, the thickness of the inner tube (t_i) must larger than t_{bk}.

7. $$f_{bk} = \frac{2{\cdot}27}{3}\frac{t_i^2 E}{D_i^2}$$

8. $$t_{bk} = \sqrt{\left(\frac{6}{2{\cdot}27}\frac{D_i^2 f_{oty} t_o}{DE}\right)}$$

Before a DSCT column fails, the concrete in the column has two confinement states as its failure mode. Han *et al.* (2010) adopted the unified concrete model suggested by Mander *et al.* (1988) and modified it. They defined the maximum strengths of confined concrete for the triaxially and biaxially confined states as in Equations 9 and 10, respectively. The adopted concrete model is represented in Figure 2(a) and by Equations 11–14 (Mander *et al.*, 1988).

9. $$f_{cc} = f_{co}\left[2{\cdot}254\sqrt{\left(1+\frac{7{\cdot}94 f_1}{f_{co}}\right)} - \frac{2f_1}{f_{co}} - 1{\cdot}254\right]$$

10. $$f_{cc} = -2{\cdot}75\frac{f_1^2}{f_{co}} + 1{\cdot}835 f_1 + f_{co}$$

11. $$f_c = \frac{f_{cc} x r}{r - 1 + x^r}$$

12. $$x = \frac{\varepsilon}{\varepsilon_{cc}}$$

13. $$r = \frac{E_c}{(E_c - E_{sec})}$$

14. $$\varepsilon_{cc} = \varepsilon_{co}\left[1 + 5\left(\frac{f_{cc}}{f_{co}} - 1\right)\right]$$

The stress–strain relation of steel was assumed to have dependence up to the yielding point. To represent perfect plasticity and nonlinearity of steel, the relation was described as a flat line from

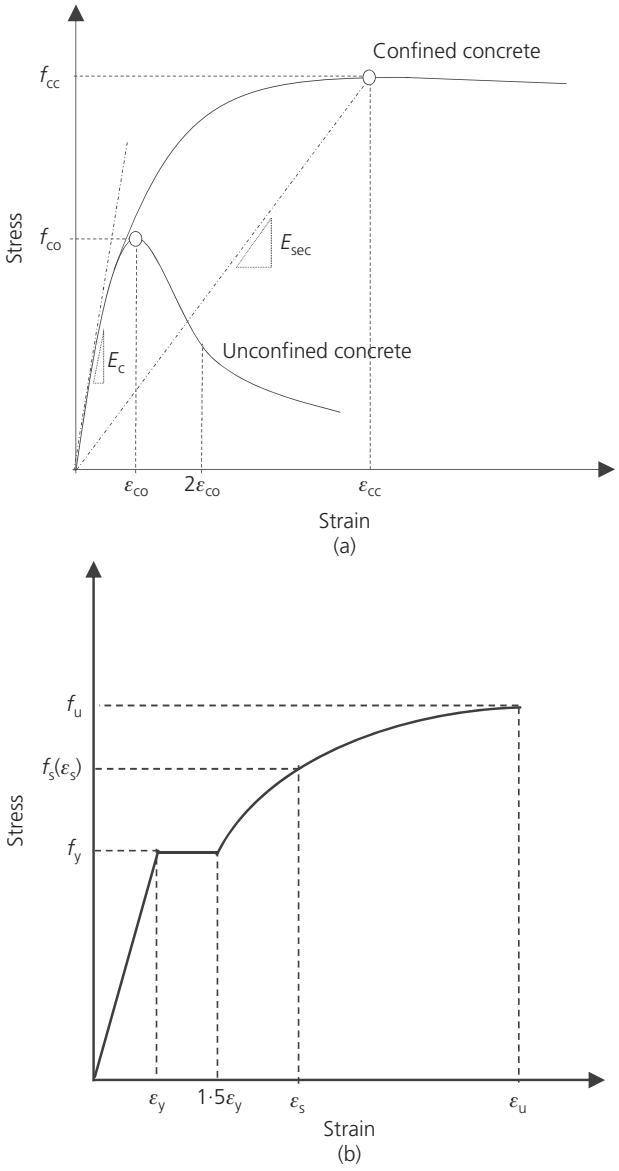

Figure 2. Applied material model

ε_y to $1{\cdot}5\varepsilon_y$ and a parabola from $1{\cdot}5\varepsilon_y$ to ε_u, as shown in Figure 2(b). The parabola is defined as in Equation 15. In mild steel, the perfectly plastic range is greater than $1{\cdot}5\varepsilon_y$.

15. $$f_s(\varepsilon_s) = f_y + (f_u - f_y)\sqrt{\left(\frac{\varepsilon_s - 1{\cdot}5\varepsilon_y}{\varepsilon_u - 1{\cdot}5\varepsilon_y}\right)}$$

Column model

The column model uses a section analysis, accounting for equilibrium, strain compatibility, material stress–strain curves and adopts the layer-by-layer technique for numerical integration of stresses (Kilpatrick and Ranagan, 1997). The analysis is

conducted for two conditions including (*a*) unconfined concrete stress–strain curve and (*b*) confined concrete stress–strain curve. Figure 3 shows the idealised section of a DSCT column. The stresses in the layers of concrete and steel tubes are calculated as the change of strain. By summing them, axial loads and moments for concrete and steel tubes are found. This analysis is performed for every step by the change of strain distribution induced by increasing lateral load as shown in Figure 4. Initially, the strain distribution starts from the zero-moment condition with the strain of ε_{cc}. Then the strain at the left side ($\varepsilon_{L,i}$) gradually decreases until the column fails. As the strain distribution changes, the distance from the neutral axis for each strain distribution ($C_{b,i}$) is given as in Equation 16. For each stage of strain distribution, stresses acting on the concrete, the inner tube and the outer tube are calculated as in Equations 17–22. By summing them, the axial load and the moment at each stage of the strain distribution are calculated as in Equations 23 and 24, respectively. When constant axial load is additionally applied, the amount of strain corresponding to the constant axial load is added to the initial strain (ε_{cc}). In this study, only the additional strain is considered by constant axial load. The P–Δ effect from large-displacement theory is not considered because the axial load was always applied parallel to the axis of the tested column by hydraulic pumps with hinges so as not to generate any moment in the experiment (Han *et al.*, 2011).

16. $$C_{b,i} = D\frac{\varepsilon_{R,i}}{\varepsilon_{R,i} - \varepsilon_{L,i}}$$

17. $$P_i^{CC} = \sum_{j=1}^{n} P_{i,j}^{CC} = \sum_{j=1}^{n} A_{i,j}^{CC} f_{i,j}^{CC}$$

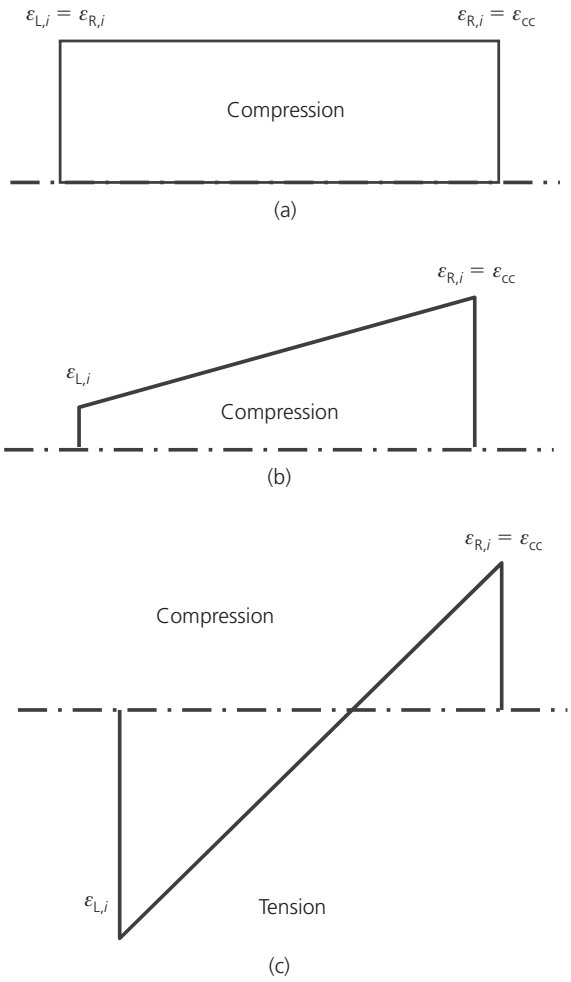

Figure 4. Stages of strain distribution: (a) initial stage; (b) middle stage; and (c) final stage

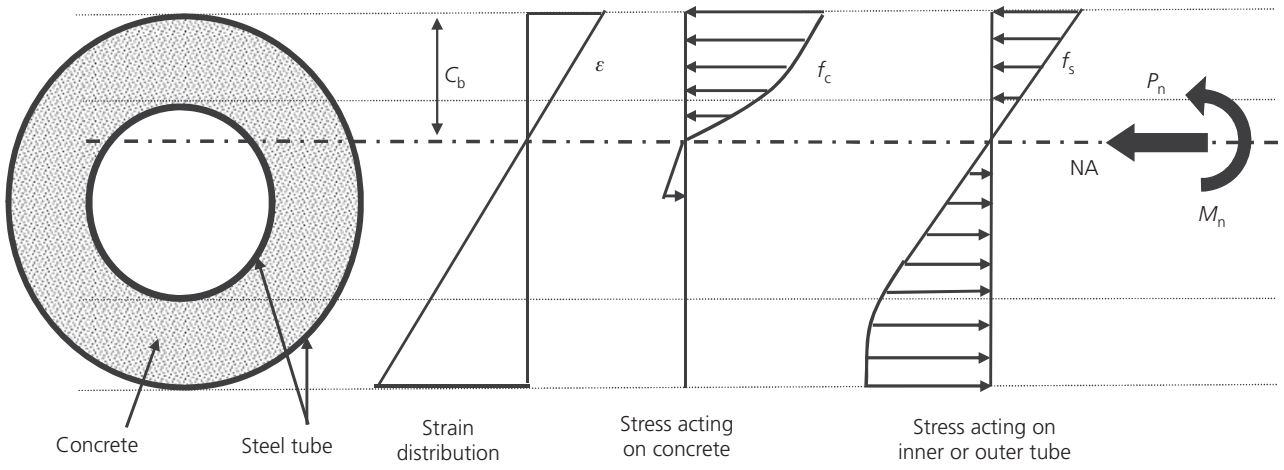

Figure 3. Section analysis using strain compatibility and layer-by-layer approach

18. $$P_i^{\mathrm{IT}} = \sum_{j=1}^{n} P_{i,j}^{\mathrm{IT}} = \sum_{j=1}^{n} A_{i,j}^{\mathrm{IT}} f_{i,j}^{\mathrm{IT}}$$

19. $$P_i^{\mathrm{OT}} = \sum_{j=1}^{n} P_{i,j}^{\mathrm{OT}} = \sum_{j=1}^{n} A_{i,j}^{\mathrm{OT}} f_{i,j}^{\mathrm{OT}}$$

20. $$M_i^{\mathrm{CC}} = \sum_{j=1}^{n} M_{\mathrm{i,j}}^{\mathrm{CC}} = \sum_{j=1}^{n} P_{i,j}^{\mathrm{CC}} x_{i,j}^{\mathrm{CC}}$$

21. $$M_i^{\mathrm{IT}} = \sum_{j=1}^{n} M_{i,j}^{\mathrm{IT}} = \sum_{j=1}^{n} P_{i,j}^{\mathrm{IT}} x_{i,j}^{\mathrm{IT}}$$

22. $$M_i^{\mathrm{OT}} = \sum_{j=1}^{n} M_{i,j}^{\mathrm{OT}} = \sum_{j=1}^{n} P_{i,j}^{\mathrm{OT}} x_{i,j}^{\mathrm{OT}}$$

23. $$P_i = P_i^{\mathrm{CC}} + P_i^{\mathrm{IT}} + P_i^{\mathrm{OT}}$$

24. $$M_i = M_i^{\mathrm{CC}} + M_i^{\mathrm{IT}} + M_i^{\mathrm{OT}}$$

Lateral forces and lateral displacements can be calculated from the determined moments and curvatures at the corresponding stages of the strain distribution. Lateral forces $F_{\mathrm{L},i}$ are simply determined by Equation 25. However, more complex calculations are required to determine the lateral displacement, Δ_i, from the curvature which is calculated using Equation 26. From the moment–curvature analysis using the section analysis, the yielding moment of the column can be determined. For the lateral load on the top of the column, the moment distribution along the column is described as shown in Figure 5. The length of the plastic hinge is given by Equation 27 for each stage (Gear and Timoshenko, 1997). The curvature is calculated by a function of z along the column height. This proposed curvature function was assumed to have a constant value in the plastic hinge zone and a parabolic relation in the elastic zone. Therefore, the curvature at any point, a distance z from the base, can be defined as in Equation 28.

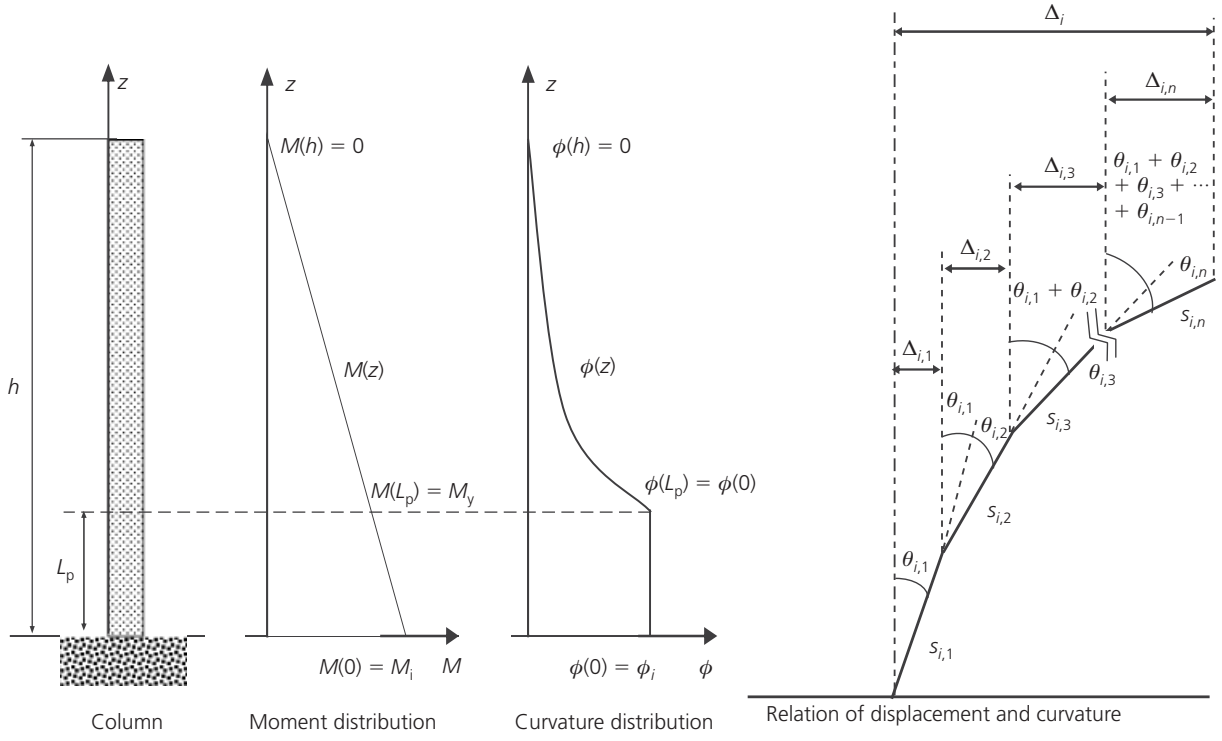

Figure 5. Curvature and displacement functions

25. $$F_{\mathrm{L},i} = \frac{M_i}{h}$$

26. $$\phi_i = \frac{\varepsilon_{\mathrm{cc}}}{C_{\mathrm{b},i}}$$

27. $$L_{\mathrm{p},i} = h\left(1 - \frac{M_{\mathrm{y}}}{M_{\mathrm{i}}}\right) \qquad (M_{\mathrm{y}} < M_{\mathrm{i}})$$

28a. $$\phi(z) = \phi_i \qquad (0 \leqslant z \leqslant L_{\mathrm{p},i})$$

28b. $$\phi(z) = \frac{\phi_i}{(h - L_{\mathrm{p},i})^2}(z - h)^2 \qquad (z > L_{\mathrm{p},i})$$

If the column is divided into numerous small elements along the column height, the curvature corresponding to each element can be calculated from the curvature function. In this study, the column was divided into 1000 elements along its height. Figure 5 shows the column composed of a certain number of elements which have the length of $S_{i,j}$. The jth element of the column has its own particular rotation angle ($\theta_{i,j}$) at the ith strain distribution. By small-displacement theory, the rotation angle is given as in Equation 29 from the curvature function and the length of the element (Gear and Timoshenko, 1997). The eventual lateral displacement ($\Delta_{i,j}$) of the jth element is affected by its rotation angle and those of previous elements. Therefore, the lateral displacement of the top point of the column can be calculated by summing the lateral displacements of all elements in the stage of the strain distribution as in Equation 30. In this study, the effect of secondary moment due to the initial axial load was not considered. Using the derived equations, a column-analysis program was coded in the Fortran language. The program judges the column to fail when one of followings happens: (*a*) the outer tube is buckled; (*b*) the strain of the outer tube reaches its ultimate value; (*c*) the axial strain of the concrete reaches its ultimate value. The buckling of the outer tube depends on Equation 31 (Korea Concrete Institute, 2007), which is proposed to determine the minimum thickness of the outer steel tube of a concrete-filled steel tube column to avoid the local buckling of the outer steel tube.

29. $$\theta_{i,j} = \phi(z) S_{i,j}$$

30. $$\Delta_i = \sum_{j=1}^{n} \Delta_{i,j} = \sum_{j=1}^{n} \left(S_{i,j} \sum_{k=1}^{j} \theta_{i,k} \right)$$

31. $$t_{\mathrm{o}} > (D_{\mathrm{o}} + t_{\mathrm{o}}) \sqrt{\left(\frac{f_{\mathrm{oty}}}{8E_{\mathrm{oty}}} \right)}$$

Verification of analytical model

The developed program was verified by comparison with experimental results. For verification of the axial strength of a DSCT column, the experimental data from Wei *et al.*'s research (Wei *et al.*, 1995a, 1995b) were used. For verification of the moment-resisting capacity of the DSCT-FT and DSCT-CT columns, the experimental results of Han *et al.* (2011) were used. The DSCT-FT column is a DSCT column having a flat inner steel tube, and the DSCT-CT column is a DSCT column having a corrugated inner steel tube; their outer tubes are steel.

Verification of axial strength

Wei *et al.* (1995a) tested the axial strength of a DSCT column and suggested an empirical model (Wei *et al.*, 1995b). They reported that the axial strength of a DSCT column is 10–30% larger than the sum of the strengths of the components: outer tube, inner tube and concrete. The verification was performed by comparing the axial strengths, analytical strength given by the developed model (N_{p}), measured strength from tests (N_{t}; Wei *et al.*, 1995a), strength from the empirical model (N_{e}; Wei *et al.*, 1995b), and strength summation of each component (N_{s}; Wei *et al.*, 1995a). For comparison, ten specimens were selected from an experimental study (Wei *et al.*, 1995b) and they are shown in Table 1. As shown in Table 1, the summation of each strength is 8–23% (average 13·38%) less than the measured axial strength. However, the developed model has only 0·4–9% (average 5·14%) error terms when compared with the measured results. This accuracy is remarkable and can be compared to an empirical model (Wei *et al.*, 1995b) which has 3·34% average error term. This means that the confining effect should be considered when a DSCT column is designed or analysed.

Verification of moment-resisting capacity

Figure 6 shows the lateral load–lateral displacement relations of the DSCT-FT and DSCT-CT column specimens by analytical results and experimental results (Han *et al.*, 2011). In the analyses, the applied lateral load was gradually increased and constant axial loads were applied. The applied axial loads to DSCT-FT and DSCT-CT columns were 1567 kN and 684 kN, which were 10% of the calculated axial strengths, respectively. The material and geometric properties of the column specimens are summarised in Table 2 and Table 3, respectively.

Figure 7 shows the strength contribution of each component in

Parameter	Specimen									
	SP-01	SP-02	SP-03	SP-04	SP-05	SP-06	SP-07	SP-08	SP-09	SP-10
D: mm	80·1	80·13	80·39	80·36	99·11	99·19	99·2	87·25	99·84	112·66
D_i: mm	63	62·94	63·84	63·33	80·85	81·17	74·62	64·66	64·55	77·24
t_i: mm	1	0·94	1·14	1·13	0·55	0·67	0·62	1·16	1·15	1·14
t_o: mm	0·9	0·87	1·11	1·14	0·59	0·71	0·7	1·55	1·56	1·64
f_{ity}: MPa	470	470	470	470	474	474	512	216	216	235
f_{oty}: MPa	524	524	524	524	409	409	409	286	255	262
E_{ity}: GPa	212	212	212	212	214	214	219	197	197	169
E_{oty}: GPa	210	210	210	210	193	193	193	209	211	195
N_t: kN[a]	330	335	386	395	283	357	380	357	477	551
N_s: kN[a]	302·75	293·86	347·75	349·56	237·82	274·62	301·59	318·75	425·89	491·96
N_e: kN[b]	339	351	384	387	302	333	371	358	452	540
N_p: kN	331·29	324·88	364·36	373·79	297·55	321·82	391·86	339·41	501·6	502·6
N_s/N_t: %	91·74	87·72	90·09	88·5	84·03	76·92	79·37	89·29	89·29	89·29
$(N_s - N_t)/N_t$: %	−8·26	−12·28	−9·91	−11·5	−15·97	−23·08	−20·63	−10·71	−10·71	−10·71
N_e/N_t: %	102·73	104·78	99·48	97·97	106·71	93·28	97·63	100·28	94·76	98
$(N_e - N_t)/N_t$: %	2·73	4·78	−0·52	−2·03	6·71	−6·72	−2·37	0·28	−5·24	−2
N_p/N_t: %	100·39	96·98	94·39	94·63	105·14	90·14	103·12	95·07	105·16	91·22
$(N_p - N_t)/N_t$: %	0·39	−3·02	−5·61	−5·37	5·14	−9·86	3·12	−4·93	5·16	−8·78

See Notation for the meaning of the symbols.
[a] Data from the research of Wei *et al.* (1995a).
[b] Data from the research of Wei *et al.* (1995b).

Table 1. Comparison of axial strength

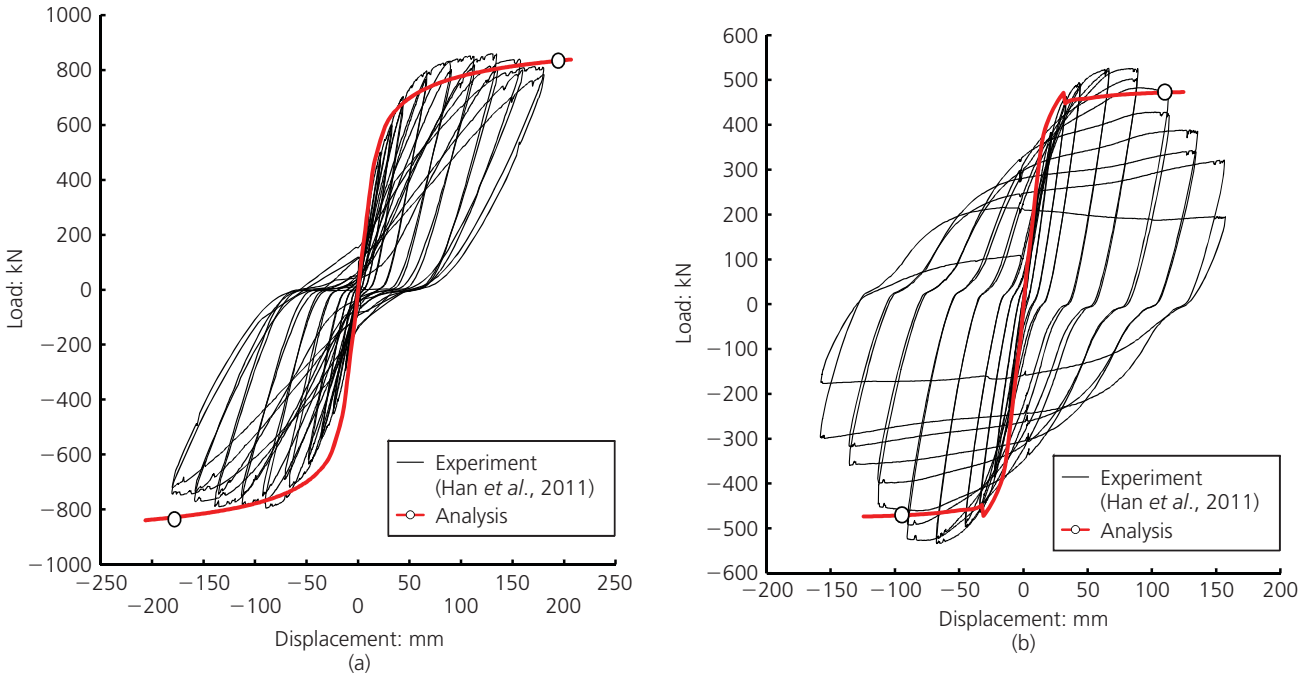

Figure 6. Experimental and analytical results: (a) DSCT-FT and (b) DSCT-CT

Material/parameter	Value
Compressive strength of unconfined concrete: MPa	21·70
Flat inner steel tube	
Yield strength: MPa	378·20
Ultimate strength: MPa	588·60
Modulus of elasticity: MPa	206 010·00
Ultimate strain	0·16
Corrugated inner steel tube	
Yield strength: MPa	206·00
Ultimate strength: MPa	274·10
Modulus of elasticity: MPa	206 010·00
Ultimate strain	0·16
Outer steel tube	
Yield strength: MPa	250·00
Ultimate strength: MPa	400·00
Modulus of elasticity: MPa	206 010·00
Ultimate strain	0·16

Table 2. Material properties of column specimens (Han *et al.*, 2010)

Parameter	Value
Column height: mm	2250
Outer diameter of confined concrete: mm	558·8
Hollow section diameter: mm	406·4
Thickness of outer steel tube: mm	10·0
Thickness of flat inner steel tube: mm	9·0
Thickness of corrugated inner steel tube: mm	2·0
Length of one-half a wave (corrugated inner steel tube)	68·0
Height of corrugation wave (corrugated inner steel tube)	13·0

Table 3. Geometric properties of column specimens (Han *et al.*, 2010)

the column specimens by analysis. In Figure 6(a), the analysis results and the experiment results (Han *et al.*, 2011) of the DSCT-FT column are compared. This shows that the developed column model predicted the behaviour of the DSCT-FT column with acceptable accuracy. In the inelastic zone of the positive-displacement region (after approximately 50 mm displacement), the analytical result showed smaller moment capacity than the experimental result from Han *et al.* (2011). But the analytical result showed larger values than the experimental result in the other zone. The analytical model overestimated the ultimate displacement of the DSCT-FT column by 14·5%. As shown in Figure 7(a), the outer steel tube primarily contributed almost 50% of the strength to the DSCT-FT column specimen. The inner steel tube and the confined concrete each contributed about 25% of the strength. Initially, the contribution of the confined concrete was much smaller than that of the inner steel tube. However, it became almost equal to that of the inner steel tube with the increase of confining stress.

Figure 6(b) shows the comparison of the experimental and analytical results of the DSCT-CT column. In the elastic region (approximately, 0 to $\pm$25 mm), the analytical model traced the actual behaviour of the column specimen with good accuracy. However, in the plastic zone, it underestimated the strength of the column specimen. As it predicted that the inner corrugated steel tube would yield before the failure of the outer steel tube, the developed program predicted that the strength of the DSCT-CT column would drop after the yield failure of the inner tube.

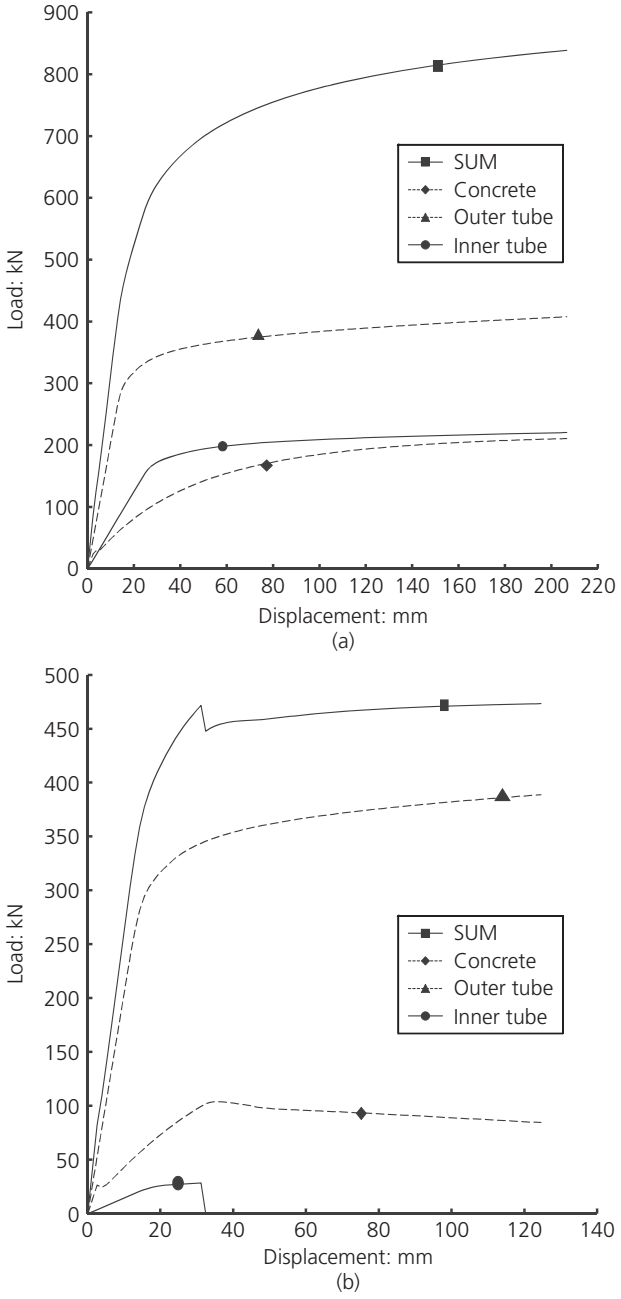

Figure 7. Strength contribution of component: (a) DSCT-FT and (b) DSCT-CT

However, this strength drop was not investigated in the test (Han *et al.*, 2011). This result can be explained by two suppositions. The first is that the inner steel tube did not yield in the test because the yielding criterion for the inner steel tube in the analytical model was conservative. And the second is that the failure of the inner steel tube had little effect upon the behaviour of the DSCT column. In effect, the experimental result says that the actual strength of the inner steel tube was higher than had been calculated by the analytical model. For this reason, the analytical model underestimated the strength of the DSCT-CT column specimen. Figure 7(b) shows the contributing portion of the each component in the DSCT-CT column specimen from the analysis result. As shown in Figure 7(b), the outer steel tube had the most part of the strength contribution to the DSCT-CT column specimen. Its contributing portion was almost 80% of the column strength. The corrugated inner steel tube contributed about 6% to the column strength before its yielding failure. However, it made no further contribution after its yielding failure. The confined concrete contributed about 22% of the column strength before the yield of the inner steel tube. However, its contributing portion was reduced to 18% by losing internal confinement after the yield failure of the inner steel tube.

In Figure 8 the lateral load–lateral displacement envelope curves of DSCT-FT and DSCT-CT column specimens are plotted from the hysteresis loops of the experimental results. Analysis results are also plotted together for comparison. The maximum loads and moments, yield and ultimate displacements, yield and ultimate energies, and energy ductility factors from the analyses and experiments are summarised in Table 4. As shown in Table 4, the analysis model predicted the strengths with an accuracy of less than 10%. The yield displacements and ultimate displacements from the experimental results (Han *et al.*, 2011) were calculated by the method suggested by Park (1988). Park defined the yield displacement and the ultimate displacement as the displacements corresponding respectively to 75% and 80% of the maximum load ($0{\cdot}75V_{max}$ and $0{\cdot}8V_{max}$). When the final load was larger than $0{\cdot}8V_{max}$, the final displacement was taken as the ultimate displacement.

The analysis model predicted yield displacements smaller than those from the experimental results. It also predicted ultimate displacements larger than those from the experimental results. These results gave analytical energy ductility factors larger than those from experimental results. However, the analytical results are acceptable for predicting the behaviour of a DSCT column.

Parametric study

A brief parametric study was carried out with the developed program for DSCT-FT columns. As the main parameters affecting the behaviour of a DSCT column, the compressive strength of concrete, the hollow ratio, and the thickness of the inner steel tube were selected. The selected parameters, their values, other dimensions and material properties are summarised in Table 5. The height of the column was set as 2500 mm. In this analysis, the initial axial loading was not considered.

Figure 9 shows the variations of P–M interaction and F–Δ curves by the variation in concrete strength (f_{co}). In these figures, t_i and the hollow ratio (D_i/D) were fixed as 5 mm and 0·7, respectively. For the parametric models, the minimum required thicknesses not to yield and not to buckle are 4·8 mm and 2·72 mm, respectively. Therefore, all the models have failure mode II as summarised in Table 6. As shown in Figure 9(a), the

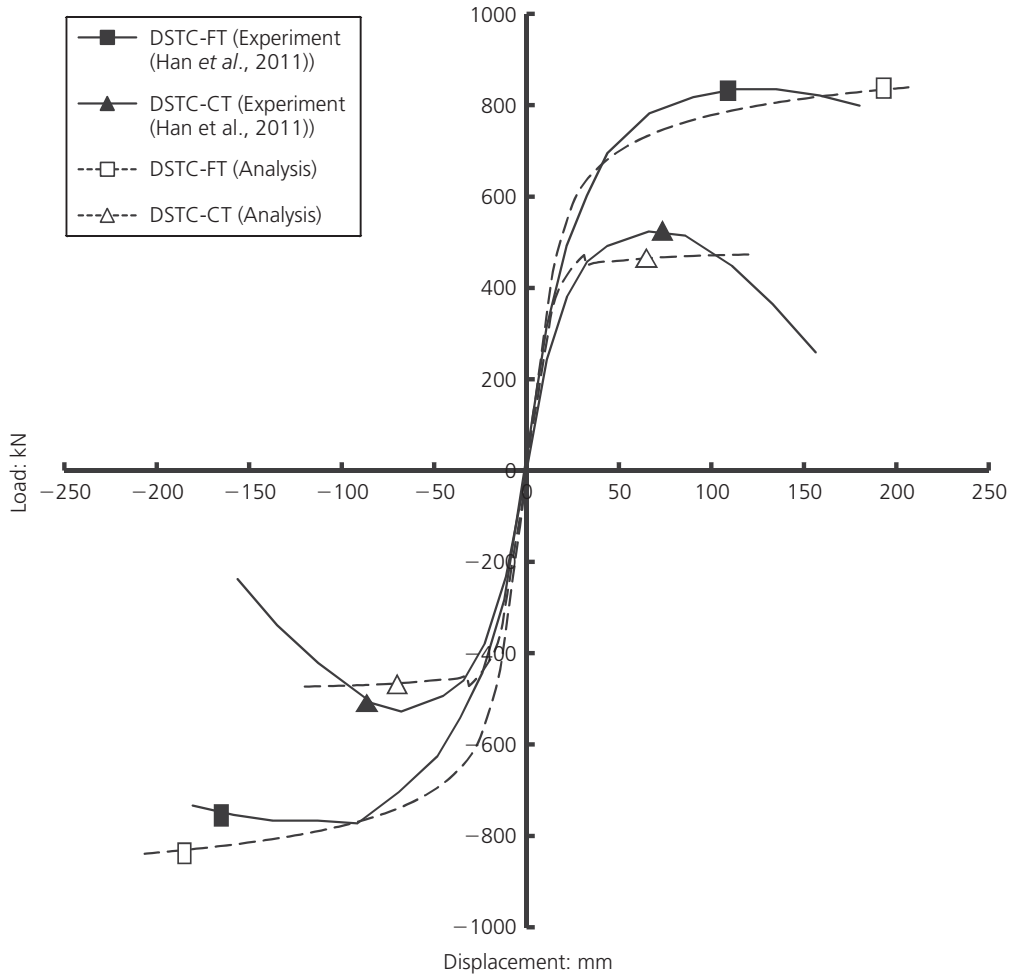

Figure 8. Comparison of envelope curves

analysis results that considered the confining effect (marked 'confined' in the figure; C-types) show higher values than those that did not (marked 'unconfined' in the figure; U-types). As the concrete strength increased, the axial strength and the moment capacity increased. However, the balanced eccentricity (e_b) decreased although P_b and M_b increased with the increase of concrete strength as shown in Table 7. This results from the concrete strength contributing more to the axial strength than to the moment capacity. In Figure 9(b), C-types show higher strengths and larger ultimate displacements than U-types. The increase in the concrete strength makes the column strength high, but it produces a small ultimate displacement as shown in Table 8. The increase in the concrete strength made the yield energy large by increasing the column strength, but it made the ultimate strength lower because of the decrease of the ultimate displacement. Therefore, the higher concrete strength produced lower ductility of the column.

Figure 10 shows the variations of P–M interaction and F–Δ curves with the variation of the hollow ratio. t_i and f_{co} were fixed as 5 mm and 25 MPa, respectively. The minimum required thicknesses are summarised in Table 6. When the hollow ratio is larger than 0·7, the test model has failure mode I. Thus, the test models with hollow ratios of 0·8 and 0·9 showed much lower axial strengths, moment capacities, and smaller displacements than the others as shown in Figure 10. The test models with failure mode II (hollow ratio = 0·5, 0·6, 0·7) showed almost equal moment capacities and ultimate displacements although they had different hollow ratios. However, they had different P_0 and P_b because they had different cross-sectional areas. As the hollow ratio increases, the cross-sectional area of the concrete decreases, but the moment of inertia of the inner tube is increased due to its enlarged diameter. This can explain why the models showed equivalent performances although they had different hollow ratios. However, the axial strength was reduced by the decrease of the cross-sectional area of the concrete.

Figure 11 shows the variation of P–M interaction curves and

Specimen		DSCT-FT	DSCT-CT
Maximum load: kN	Analysis	839·01	473·41
	Experiment	801·10	523·63
	Ratio (%)	104·7	90·4
Maximum moment: kN	Analysis	1887·77	1065·18
	Experiment	1802·48	1178·17
	Ratio (%)	104·7	90·4
Yield displacement: mm	Analysis	41·14	19·02
	Experiment	51·00	32·00
	Ratio (%)	80·7	59·43
Ultimate displacement: mm	Analysis	206·50	124·49
	Experiment	180·38	119·00
	Ratio (%)	114·5	104·6
Ultimate energy: kN m	Analysis	149·04	53·42
	Experiment	123·25	51·39
	Ratio (%)	120·9	103·95
Yield energy: kN m	Analysis	19·31	4·71
	Experiment	22·58	8·46
	Ratio (%)	85·5	55·7
Energy ductility factor	Analysis	7·72	11·34
	Experiment	5·46	6·07
	Ratio (%)	141·4	186·8

The DSCT-FT column is a DSCT column having a flat inner steel tube; the DSCT-CT column is a DSCT column having a corrugated inner steel tube.

Table 4. Comparison of analysis and test results

F–Δ curves with the variation of t_i. The hollow ratio and f_{co} were fixed as 0·7 and 25 MPa, respectively. As summarised in Table 6, the minimum required thicknesses are 4·8 mm and 2·72 mm for the yielding and buckling conditions, respectively. Therefore, test models with the thicknesses of 1 mm and 3 mm have failure mode I, and the others have failure mode II. Enlarging t_i increases the cross-sectional area and the moment of inertia of the inner tube, and these increase the axial strength and moment capacity of the column as shown in Figure 11(a) and Table 7. This could provide a solution to enhancing the performance of a DSCT column without increasing its outer diameter. It also increased the ultimate displacement and ductility of the DSCT column as shown in Figure 11(b) and Table 8.

Conclusions

In this study, an analytical model of a DSCT column was proposed, and an analysis program was developed. The developed analysis program was verified with the experimental results. The analysis program shows a P–M interaction curve, an F–Δ curve, yield displacement, ultimate displacement, yield energy, and ultimate energy. Using the developed analysis program, a parametric study was performed. Based on the results of this parametric study, the following conclusions are drawn.

(*a*) The analytical model was verified with experimental results and it predicted the behaviour of a DSCT column with acceptable accuracy. It overestimated the strength of the DSCT-FT column by 4·7%, and underestimated the strength of the DSCT-CT column by 9·6%. It overestimated the ultimate displacements of the DSCT-FT and DSCT-CT columns by 14·5% and 4·6%, respectively.

(*b*) The high strength of concrete produces high axial strength and large moment capacity of a DSCT column. However, its balanced eccentricity decreased because the concrete strength contributes more to the axial strength than to the moment capacity. The increase of the concrete strength gives the column low ductility because it provides the large yield energy and small ultimate displacement.

(*c*) DSCT columns have almost equal moment capacities and ultimate displacements although they have different hollow ratios if they have failure mode II. This is because the increase of the hollow ratio reduces the cross-sectional area of the concrete, but it enlarges the diameter of the inner tube. However, the axial strength of a DSCT column is reduced by the reduction of the cross-sectional area of the concrete.

(*d*) The outer tube contributes most to the moment capacity of a DSCT column. Therefore, the simplest method to enhance the performance of a DSCT column is to give it a thick outer tube. However, unnecessarily making t_o large is not economic

	Outer steel tube	Inner steel tube	Concrete	Hollow ratio
Outer diameter: mm	500	250, 300, 350, 400, 450	—	0·5, 0·6, 0·7, 0·8, 0·9
Thickness: mm	8	1, 3, 5, 7, 9	—	
Yield strength: MPa	300	350	—	
Ultimate or maximum strength: MPa	450	500	20, 23, 25, 27, 30	
Modulus of elasticity: MPa	210 000	210 000	—	
Ultimate strain	0·16	0·16	0·003	

Table 5. Geometric and material properties

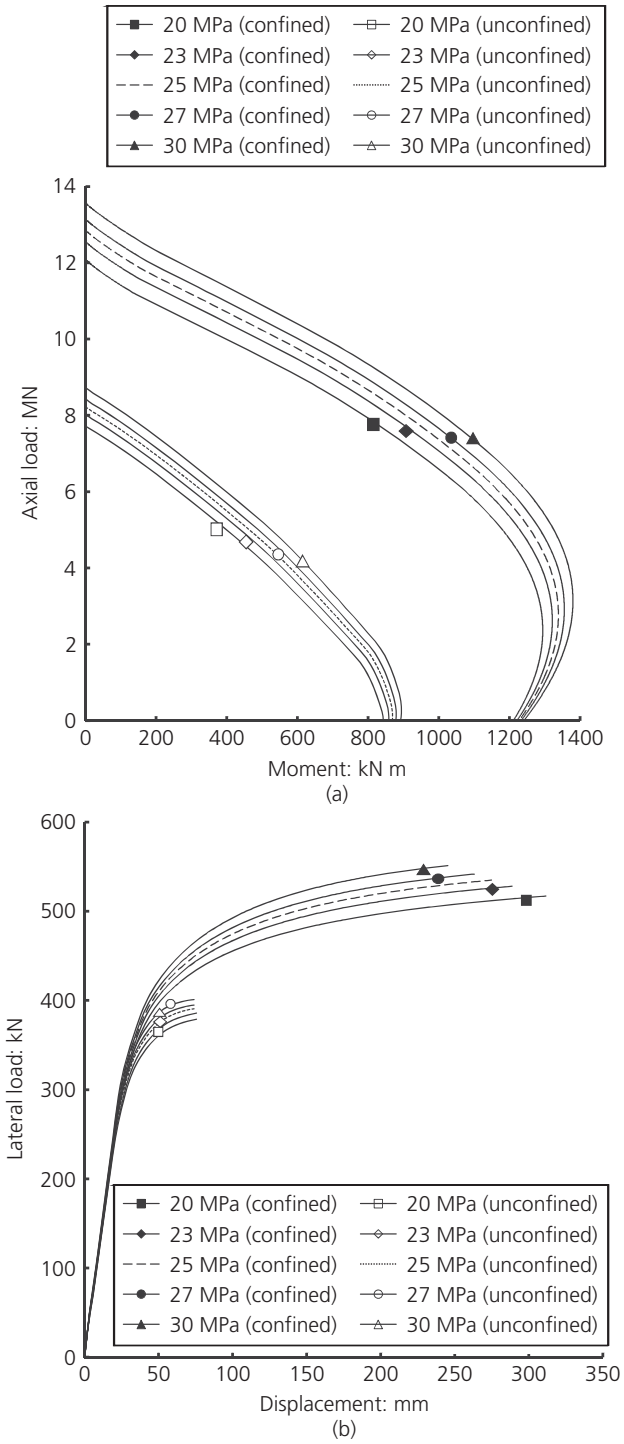

Figure 9. Column behaviour by concrete strength ($t_i = 5$mm, hollow ratio = 0·7): (a) P–M interaction curve and (b) F–Δ curve

Model			t_{yt}: mm	t_{bk}: mm	Failure mode
t_i:mm	D_i/D	f_{co}: MPa			
5	0·7	20	4·800	2·720	II
5	0·7	23	4·800	2·720	II
5	0·7	25	4·800	2·720	II
5	0·7	27	4·800	2·720	II
5	0·7	30	4·800	2·720	II
5	0·5	25	3·428	1·943	II
5	0·6	25	4·114	2·332	II
5	0·8	25	5·486	3·109	I
5	0·9	25	6·171	3·498	I
1	0·7	25	4·800	2·720	I
3	0·7	25	4·800	2·720	I
7	0·7	25	4·800	2·720	II
9	0·7	25	4·800	2·720	II

See Notation for the meaning of the symbols.

Table 6. Required minimum thickness of the inner tube

Model			P_0: kN	M_0: kN m	P_b: kN	M_b: kN m	e_b: mm
t_i: mm	D_i/D	f_{co}: MPa					
5	0·7	20	12 091	1210	2428	1293	533
5	0·7	23	12 558	1220	2606	1320	507
5	0·7	25	12 857	1226	2778	1337	482
5	0·7	27	13 146	1231	2915	1354	465
5	0·7	30	13 568	1239	3146	1379	438
5	0·5	25	15 196	1137	4239	1354	320
5	0·6	25	14 150	1184	3582	1352	378
5	0·8	25	9913	1104	1259	1137	903
5	0·9	25	8356	1096	406	1100	2705
1	0·7	25	7624	764	723	784	1085
3	0·7	25	9526	927	1396	974	697
7	0·7	25	13 697	1324	2736	1424	520
9	0·7	25	14 528	1418	2735	1508	552

See Notation for the meaning of the symbols.

Table 7. Balanced load and moment

because t_i should be enlarged to induce failure mode II of the DSCT column.

(*e*) Enlarging t_i gives high axial strength and large moment capacity of a DSCT column. This could be a solution to enhancing the performance of a DSCT column without increasing its outer diameter. It also increases the ductility of the DSCT column.

Acknowledgements

This research was financially supported by the Korea Institute of Ocean Science and Technology (KIOST), project no. PE98817.

Model			Energy ductility factor			Displacement ductility factor		
t_i: mm	D_i/D	f_{co}: MPa	Yield energy: kN m	Ultimate energy: kN m	Ductility factor	Yield displacement: mm	Ultimate displacement: mm	Ductility factor
5	0·7	20	17·4	139·1	7·975	60·3	311·6	5·170
5	0·7	23	18·3	130·6	7·145	62·0	288·6	4·655
5	0·7	25	18·4	125·2	6·811	61·8	274·8	4·448
5	0·7	27	18·5	120·8	6·517	61·6	263·1	4·267
5	0·7	30	18·6	113·6	6·098	61·2	245·3	4·009
5	0·5	25	22·3	120·8	5·416	72·4	266·7	3·686
5	0·6	25	20·3	123·1	6·059	67·0	270·0	4·031
5	0·8	25		Brittle failure			Brittle failure	
5	0·9	25		Brittle failure			Brittle failure	
1	0·7	25		Brittle failure			Brittle failure	
3	0·7	25		Brittle failure			Brittle failure	
7	0·7	25	19·7	134·2	6·825	62·1	276·4	4·448
9	0·7	25	20·0	142·3	7·117	60·0	276·4	4·607

See Notation for the meaning of the symbols.

Table 8. Energy and displacement ductility

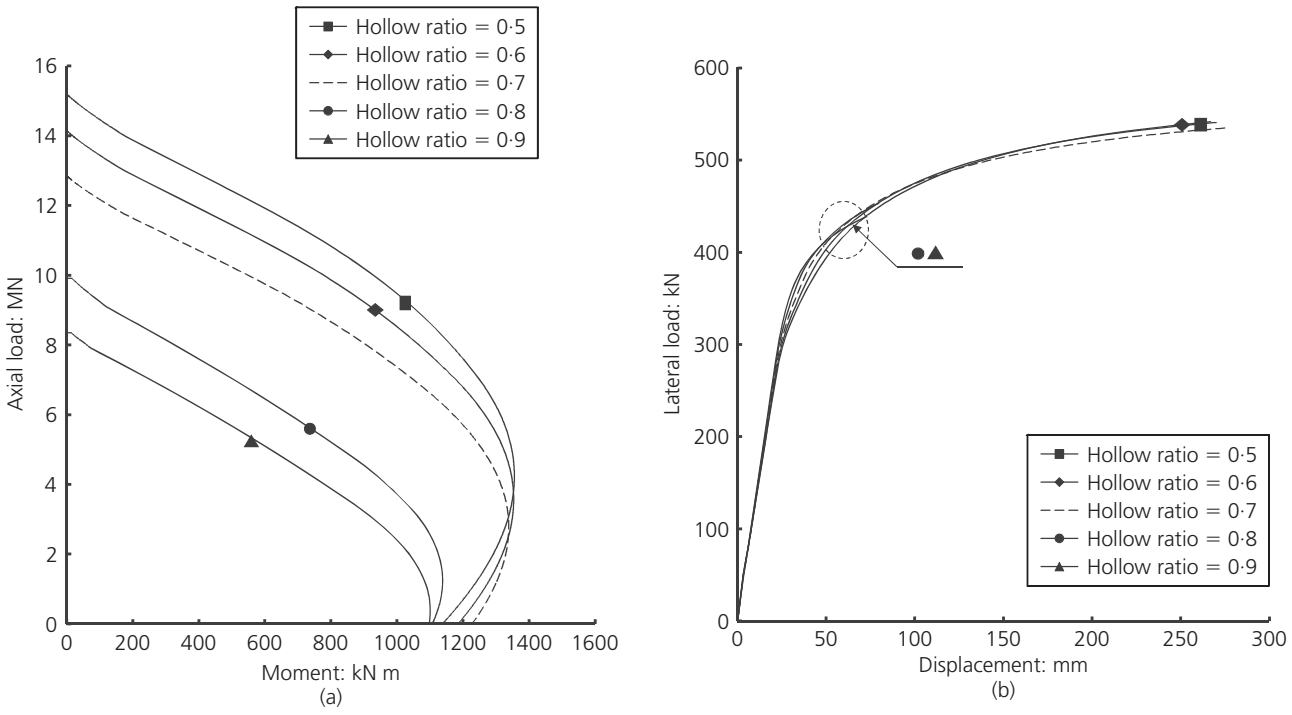

Figure 10. Column behaviour by hollow ratio ($t_i = 5$ mm, $f_{co} = 25$ MPa): (a) P–M interaction curve and (b) F–Δ curve

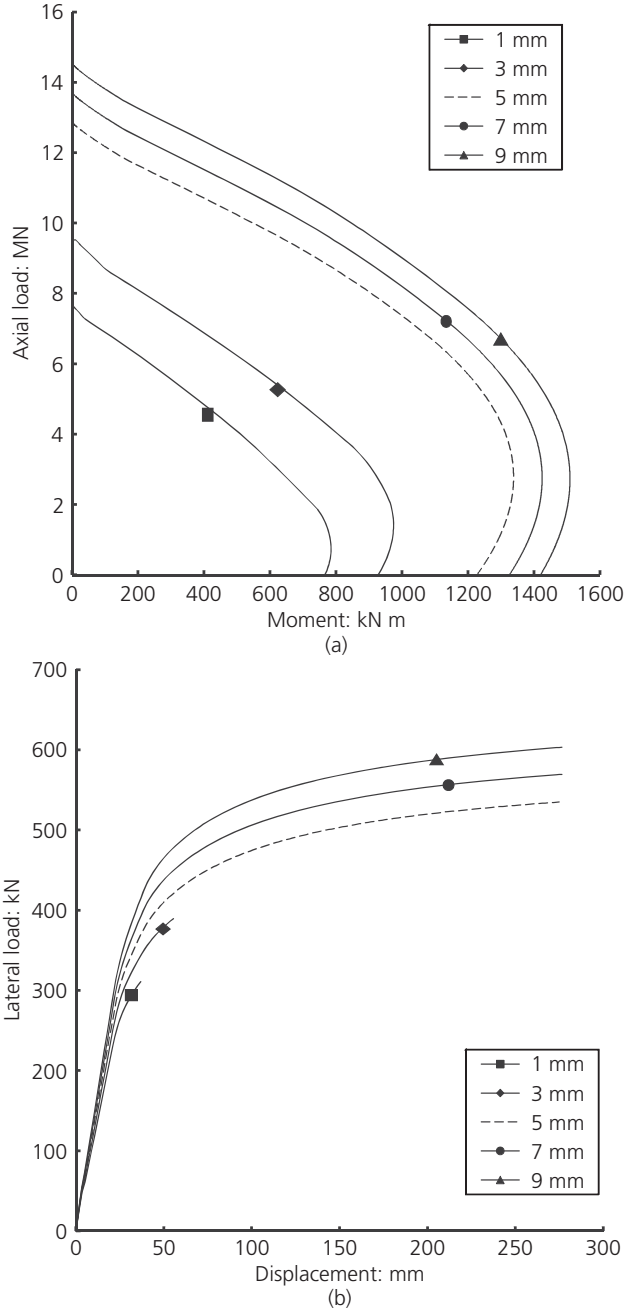

Figure 11. Column behaviour by thickness of the inner tube ($f_{co} = 25$ MPa, hollow ratio = 0·7)

REFERENCES

Gear JM and Timoshenko SP (1997) *Mechanics of Materials*, 4th edn. PWS Publishing Company, Boston, USA.

Han TH, Stallings JM and Kang YJ (2010) Nonlinear concrete model for double-skinned composite tubular columns. *Construction and Building Materials* **24(12)**: 2542–2553.

Han TH, Kim JS, Won DH and Kang YJ (2011) Experimental study on lateral behavior of DSCT Column. *Proceedings of the 6th International Conference on Asian and Pacific Coasts, Hong Kong, China*, 2100–2107.

Kerr AD and Soifer MT (1969) The linearization of the prebuckling state and its effects on the determined instability load. *Journal of Applied Mechanics* **36(3)**: 775–785.

Kilpatrick AE and Ranagan BV (1997) *Deformation-Control Analysis of Composite Concrete Columns*. Research Report no. 3/97. School of Civil Engineering, Curtin University of Technology, Perth, Western Australia.

Korea Concrete Institute (2007) *Design Specifications for Concrete Structures*. Korea Concrete Institute, Seoul, Korea

Mander JB, Priestley MJN and Park R (1988) Theoretical stress–strain model for confined concrete. *Journal of the Structural Division, ASCE* **114(8)**: 1804–1826.

Park R (1988) Ductility evaluation from laboratory and analytical testing. *Proceedings of the 9th World Conference on Earthquake Engineering, Tokyo, Japan*, **8**, 605–616.

Tao Z, Han LH and Zhao XL (2004) Behavior of concrete-filled double skin (CHS inner and CHS outer) steel tubular stub columns and beam columns. *Journal of Constructional Steel Research* **60**: 1129–1158.

Teng JG, Yu T, Wong YL and Dong SL (2006) Hybrid FRP–concrete–steel tubular columns: concept and behavior. *Construction and Building Materials* **21(4)**: 846–854.

Wei S, Mau ST, Vipulanandan C and Mantrala SK (1995a) Performance of new sandwich tube under axial loading: experiment. *Journal of Structural Engineering* **121(12)**: 1806–1814.

Wei S, Mau ST, Vipulanandan C and Mantrala SK (1995b) Performance of new sandwich tube under axial loading: analysis. *Journal of Structural Engineering* **121(12)**: 1815–1821.

Yu T, Wong YL, Teng JG, Dong SL and Lam ESS (2006) Flexural behavior of hybrid FRP-concrete-steel double-skin tubular members. *Journal of Composites for Construction, ASCE* **10(5)**: 443–452.

Zhao XL and Grzebieta R (2002) Strength and ductility of concrete filled double skin (SHS inner and SHS outer) tubes. *Thin-Walled Structures* **40(2)**: 199–213.

WHAT DO YOU THINK?

To discuss this paper, please submit up to 500 words to the editor at www.editorialmanager.com/macr by 1 July 2013. Your contribution will be forwarded to the author(s) for a reply and, if considered appropriate by the editorial panel, will be published as a discussion in a future issue of the journal.